RSC Advances

PAPER

View Article Online
View Journal | View Issue

Cite this: *RSC Adv.*, 2017, **7**, 11355

Shell thickness-dependent antibacterial activity and biocompatibility of gold@silver core–shell nanoparticles†

Longping Yang,[a] Wenjing Yan,*[a] Hongxia Wang,[a] Hong Zhuang[b] and Jianhao Zhang*[a]

Received 12th January 2017
Accepted 6th February 2017

DOI: 10.1039/c7ra00485k

rsc.li/rsc-advances

Antimicrobial activity of silver is highly effective and broad-spectrum; however, poor long-term antibacterial efficiency and cytotoxicity toward mammalian cells have restricted their applications. Here, we fabricated Au@Ag NPs with tailored shell thickness, and investigated their antibacterial activities against both Gram-negative bacteria (*Escherichia coli*) and Gram-positive bacteria (*Staphylococcus aureus*) and the cytotoxicity toward SH-SY5Y human cells, for the first time. Our results demonstrate that Au@Ag NPs with a thickness of 5 nm or Au : Ag ratio 1 : 1 (Au@Ag-2 NPs) have the highest antibacterial activity and excellent biocompatibility. The minimum inhibitory concentration (MIC) values of Au@Ag-2 NPs in terms of effective silver concentration are 5 μg mL^{-1} for *E. coli* and 7.5 μg mL^{-1} for *S. aureus*, which is significant lower than that of Ag NPs or the simple mixture of Ag and Au NPs and suggests the synergistic effects of Au and Ag in core–shell NPs. Live/dead bacterial assay and scanning electron microscope (SEM) images demonstrated that the Au@Ag NPs disrupt the bacterial cell membrane which subsequently results in cellular material leakage and cell death. The Au@Ag NPs may have great potential as effective antibacterial agents for pathogen control in hospitals and food processing.

Introduction

To cope with the overwhelming challenges of infectious diseases resulting from pathogenic bacteria, nano-sized materials, emerging as new types of safe and cost-effective bactericidal materials, have been widely investigated. Among those numerous nanomaterials, silver nanoparticles (Ag NPs) are the most promising antibacterial agents because of their inherent properties of high thermal stability, limited microbial resistance, and broad-spectrum antimicrobial activity against bacteria, viruses and other eukaryotic microorganisms.[1–4] Sondi and co-workers[5] demonstrated that Ag NPs can easily adsorb to the membrane surface of bacteria through electrostatic interaction, form permeable pits, and cause an osmotic collapse in the cells. The other possible mechanism is the release of silver ions (Ag^+) from the oxidized Ag NPs.[6–8] Ag NPs are easy to oxidize and produce a high concentration of Ag^+, the released Ag^+ then destroys the respiratory chain and leads to the formation of reactive oxygen species (ROS), such as hydroxyl radicals, H_2O_2 and hydroperoxyl radicals, which finally trigger cell damage of the cellular components and leads to the death of the bacteria.[9–11] In spite of this, the easy oxidation of pure Ag NPs and the toxicity in mammalian cells remain challenges in Ag NP applications.[12–14]

To address this problem, Ag NPs have been decorated with other nanomaterials by the formation of nanostructures. Song *et al.*[15] synthesized the silver/polyrhodanine composite-decorated silica nanoparticles, which exhibited excellent antimicrobial activity toward *Escherichia coli* (*E. coli*) and *Staphylococcus aureus* (*S. aureus*) because of the antibacterial effects of both the silver nanoparticles and the polyrhodanine. Tan *et al.*[16] synthesized antibacterial Ag@dsDNA@GO, which can wrap around the *Xanthomonas perforans* cell and results in rapid cell apoptosis, showing the synergistic antibacterial effect. While these nanostructures can effectively enhance the antibacterial activity of Ag NPs, they often require complex and tedious preparation methods, and suffering from low yields, poor long-term antibacterial activity, and biocompatibility problems.[17,18]

Bimetallic core–shell nanoparticles are gradually attracting more and more attention in recent years, because of their unique electronic, optical, chemical, and catalytic properties.[19–24] These properties are distinct and superior to their constituent monometallic elements due to the new synergistic effects. Furthermore, core–shell nanoparticles are highly functional materials with modified properties. By changing the constituting core or shell materials, the properties of the overall particle such as thermal stability, antibacterial activity, and cytotoxicity can be

[a]*National Center of Meat Quality & Safety Control, College of Food Science and Technology, Nanjing Agricultural University, Nanjing, Jiangsu 210095, China*
[b]*Quality and Safety Assessment Research Unit, Agricultural Research Service, USDA, Athens, GA 30605, USA. E-mail: ywj1103@njau.edu.cn; nau_zjh@njau.edu.cn*

† Electronic supplementary information (ESI) available: Characterization data for TEM, size distribution by DLS, UV-Vis spectra, visual color change of NPs; ICP-MS results for Au@Ag NPs; percentage of dead bacteria of bacteria after treatments with NPs, absorption spectra of NPs used for stability comparison; antibacterial assessment of different nanoparticles solution. See DOI: 10.1039/c7ra00485k

tailored.[25–28] Au NPs have advantages of easy preparation, homogeneity and biocompatibility, but suffer from low antibacterial property. Madhuchanda Banerjee *et al.*[29] fabricated bimetallic Au@Ag NPs with positive charges on the surface. This structure showed enhanced antibacterial activity against both Gram negative and Gram positive bacteria at low concentration of silver present in the shell. The MIC values in terms of effective silver concentration in core–shell NPs are much lower than that of Ag NPs, indicating that their bactericidal efficiency was much higher than that of similar sized Ag NPs. However, the influence of shell thickness of Au@Ag NPs on antibacterial activities and toxicity have not been studied, and the antibacterial mechanism is still not very clear. Because the size, surface charge and coating of NPs play a significant role in the antibacterial properties, it is necessary to control the thickness of the silver shell to obtain excellent antibacterial activity against bacteria and low toxicity to healthy human cells.[30]

Here, we synthesize high yields of Au@Ag NPs with a fixed diameter of gold core and a tunable shell thickness using poly(vinyl pyrrolidone) (PVP) as stabilizing agent. Gram-negative bacteria *E. coli* and Gram-positive bacteria *S. aureus* as model bacteria were used to investigate antibacterial activities of the Au@Ag NPs. We studied the influence of the thickness of silver shell and the dosages of Au@Ag NPs on their bioactivities. The minimum inhibitory concentration (MIC) of Au@Ag NPs was also evaluated to qualitatively estimate the antibacterial efficiency. In parallel, Au NPs, Ag NPs, and the simple mixture of Ag NPs and Au NPs at the same concentration were used as controls for comparison. The biocompatibility of Au@Ag NPs toward mammalian cells (SH-SY5Y) were evaluated using MTT assay and the antibacterial mechanism of Au@Ag NPs were measured using the live/dead assay and the SEM images.

Results and discussion

Characterization of gold@silver core–shell nanoparticles

In this study, the bimetallic Au@Ag NPs were synthesized by deposition of Ag^+ on the surface of gold core nanoparticles (10 nm) and then reduced by sodium ascorbate to form Ag shell, in the meantime, PVP was used as stabilizing agent binding to the surface of Au@Ag NPs. Transmission electron microscopy (TEM) images revealed that the prepared Au@Ag NPs were monodispersed and exhibited distinct variation in contrast between the dark gold core and the lighter silver shell (Fig. 1A–D and S1, ESI†). Statistical analysis of as many as 200 images indicated that the yield for the prepared Au@Ag NPs was as high as 98%. Besides, for three types of Au@Ag NPs, with the increase in the concentration of Ag^+ ions, the shell thickness was increased. Based on the results of inductively coupled plasma mass spectrometry (ICP-MS) (Table S1, ESI†), the content of silver in Au@Ag-1, Au@Ag-2, and Au@Ag-3 NPs was 2.6 μg mL^{-1}, 4.0 μg mL^{-1}, 15.5 μg mL^{-1}, respectively, and the Au/Ag ratio was 3 : 2, 1 : 1, and 1 : 4, respectively.

Hydrodynamic diameters of Au@Ag NPs with different thickness was determined by dynamic light scattering (DLS) (Fig. S2A, ESI†). With the increase in the concentration of $AgNO_3$, the diameter of Au@Ag NPs was increased from 13.5 to 28.2 nm, the average shell thickness of Au@Ag-1, Au@Ag-2, and Au@Ag-3 NPs were 1.5 nm, 5.0 nm, and 8.8 nm, respectively, (Fig. S2B, ESI†) based on DLS spectrum, which are in agreement with the statistical results of TEM images. Zeta potential of Au@Ag NPs was measured to be −5 mV using dynamic light scattering (results not shown). For the colloid solution, with the increased of the concentration of $AgNO_3$, the color changed from original red (Au NPs) to yellow depending on the extent of coverage of Ag atoms on the surface of Au NPs (Fig. S2C, ESI†). The UV-Vis spectra of Au NPs and Ag NPs showed an absorbance peak at 520 nm and 400 nm, respectively, corresponding to a pure monometallic NPs. Au@Ag NPs showed double peaks at 400 nm and 500 nm, and the absorbance increased as the shell thickness increased, which consists with previous reports (Fig. S2D, ESI†).[31,32]

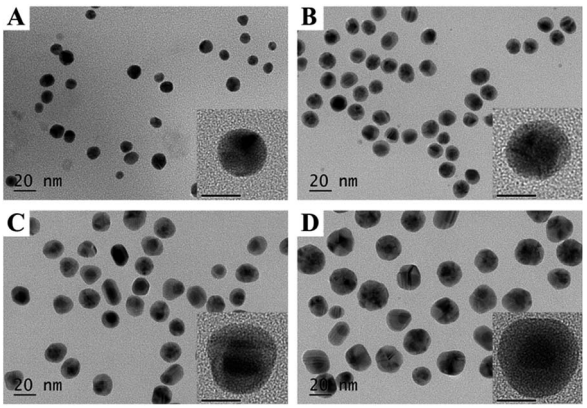

Fig. 1 TEM and high-resolution TEM (inset) images of (A) Au NPs, (B) Au@Ag-1 NPs, (C) Au@Ag-2 NPs, (D) Au@Ag-3 NPs. The scale bars in high-resolution TEM images represent 10 nm.

Shell thickness-dependent antibacterial activity of gold@silver core–shell nanoparticles

To investigate the influence of shell thickness of Au@Ag NPs on the antibacterial activity, we treated *E. coli* (Gram-negative bacteria) and *S. aureus* (Gram-positive bacteria) suspensions with three types of the synthetic Au@Ag NPs at different concentrations. The content of Au@Ag NPs was expressed by the total concentration of Ag and Au measured by ICP-MS. As shown in Fig. 2A and B, all NPs exhibited dose-dependent antibacterial activity against *E. coli* and *S. aureus*, the percent of dead bacteria was increased with the increase in the concentration of NPs. Furthermore, for three types of core–shell NPs, Au@Ag-2 NPs with the shell thickness of 5 nm and Au@Ag-3 NPs with the shell thickness of 8.8 nm showed the higher antibacterial activity compared with Au@Ag-1 NPs at the same concentration. Specifically, Au@Ag-2 NPs at the concentration of 5 μg mL^{-1} killed 99% *E. coli* and 97% *S. aureus*.

We further studied the growth kinetics of *E. coli* and *S. aureus* in liquid media after treatment with Au@Ag NPs. The bacterial proliferation was monitored by measuring the optical density at 600 nm (OD_{600}) within 24 h. Compared with the control group, the growth curve in the presence of Au@Ag NPs showed an

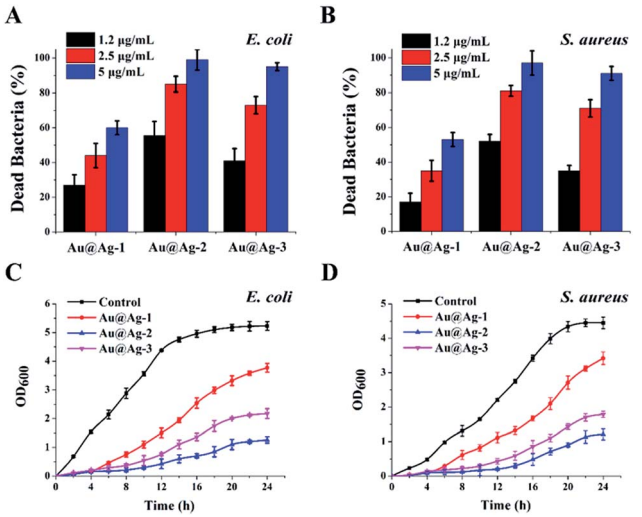

Fig. 2 Percentage of dead bacteria of (A) *E. coli* and (B) *S. aureus* after treatment with three types of Au@Ag NPs at 37 °C for 24 h, the growth curves of (C) *E. coli* and (D) *S. aureus* obtained by culturing bacteria in broth medium containing 5 μg mL^{-1} Au@Ag NPs. Error bars represent the standard deviations ($n \geq 4$).

extended lag phase, suggesting the inhibition of proliferation of *E. coli* and *S. aureus*. Among the three types of bimetallic Au@Ag NPs, the Au@Ag-2 NPs displayed a highest antibacterial activity during the whole time period regardless of NPs concentration and bacterial type. This result is interesting because compared with Au@Ag-3, the Au@Ag-2 NPs had lower content of Ag, yet still exhibited a significantly higher antibacterial activity than that of Au@Ag-3 NPs. We speculated that this might result from smaller size of Au@Ag-2 NPs or larger ratio of surface area over volume.[33] Here, the calculated specific surface area are 0.44 for Au@Ag-1 NPs, 0.39 for Au@Ag-2 NPs and 0.21 for Au@Ag-3 NPs, respectively. Au@Ag-2 NPs have higher specific surface area and may have faster Ag^+ release rate compared with larger Au@Ag-3 NPs. It has been reported that the release rate of Ag^+ had a significant effect on the antibacterial efficiency of Au@Ag NPs.[34]

To test this hypothesis, we measured the concentration of Ag^+ releasing from Au@Ag NPs solution incubated with *E. coli* at various time. As shown in Fig. 3, Au@Ag NPs with different sizes exhibited different release rate of Ag^+. Au@Ag-1 NPs showed the fastest release rate, the concentration of Ag^+ in solution reached to 0.57 μg mL^{-1} (maximum) after 6 h and 1.24 μg mL^{-1} (maximum) Ag^+ was released from the Au@Ag-2 NPs after 12 h; however, though the content of silver in Au@Ag-3 NPs is the highest, they exhibited the slowest release rate of Ag^+, only 1.2 μg mL^{-1} Ag^+ was released after 24 h. Our results here demonstrate that the antibacterial activity of Au@Ag NPs is not only related to the content of silver in nanoparticles, but also related to the rate and extent of Ag^+ release. Compared with the other two NPs, although the Au@Ag-2 NPs with 5 nm Ag shell thickness have a moderate concentration of Ag^+, it releases the most content of Ag^+ in 24 h, thus exhibiting the highest antibacterial activity during 24 h incubation. In follow-up studies, we explored antibacterial mechanisms of Au@Ag NPs with the

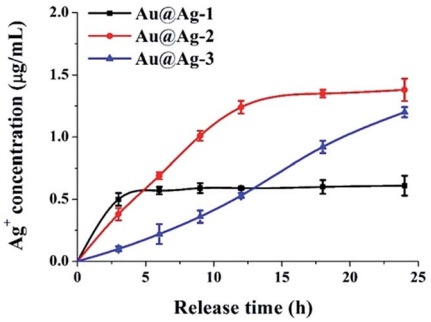

Fig. 3 The cumulative Ag^+ release profile of Au@Ag NPs (at 5 μg mL^{-1}) at various time points after treatment with *E. coli*.

example of Au@Ag-2 NPs since it showed the best antibacterial activities among three synthesized Au@Ag NPs.

Synergistic antibacterial activity of gold@silver core–shell nanoparticles

In order to better understand the enhanced antibacterial activity of Au@Ag NPs, bacteria cells were treated with different concentrations of various NPs, including pure Au NPs (10 nm), pure Ag NPs (10 nm), the mixture of Au and Ag NPs (Au : Ag = 1 : 1), and Au@Ag-2 NPs. The percentage of dead bacteria was recorded, as shown in Fig. S4 (ESI†). Results showed that the percentage of dead bacteria of *E. coli* and *S. aureus* after treatment with Au@Ag NPs was obviously higher than that of the other NPs at the same concentration, suggesting that Au@Ag NPs have the highest antibacterial activity than that of pure Au NPs, pure Ag NPs and the simple mixture of Au and Ag NPs.

We further performed the minimum inhibitory concentration (MIC) test to quantitatively compare the antibacterial property of the Au@Ag-2 NPs and other NPs, the total metal concentrations of each NPs was calculated based on the mass ratios determined by ICP-MS. From the results shown in Table 1, it can be summarized as follows: first, the MIC for the Au@Ag-2 NPs were 10 μg mL^{-1} for *E. coli* and 15 μg mL^{-1} for *S. aureus*, which in terms of effective silver concentration were 5 μg mL^{-1} for *E. coli* and 7.5 μg mL^{-1} for *S. aureus*. These values are

Table 1 Minimum inhibitory concentrations of nanoparticles against *E. coli* and *S. aureus*

		Concentration in MIC value (μg mL^{-1})		
Bacterial strain	Samples	Total	Ag	Au
E. coli (ATCC25922)	Au@Ag-2	10	5	5
	Ag + Au	30	15	15
	Ag NPs	15	15	—
	Au NPs	>500	—	>500
S. aureus (CMCC(B)26003)	Au@Ag-2	15	7.5	7.5
	Ag + Au	36	18	18
	Ag NPs	20	20	—
	Au NPs	>500	—	>500

significantly lower than that of pure Ag NPs (15 μg mL^{-1} for *E. coli* and 20 μg mL^{-1} for *S. aureus*, respectively), indicating that Au@Ag NPs have significantly higher antibacterial activity than Ag NPs by themselves. Second, the MIC for the Au@Ag-2 NPs was much lower than that of the mixture of Au and Ag NPs, suggesting that the antibacterial activity of Au@Ag NPs is not simply the additive effects of Au NPs and Ag NPs. Third, *E. coli* is more sensitive to Au@Ag-2 NPs than that of *S. aureus*, which was attributed to the difference in the cell wall constituents between Gram-negative and Gram-positive bacteria. It has been shown that the Au@Ag NPs are more readily to penetrate and impair the thinner peptidoglycan layer in Gram-negative bacteria cells.[35]

The Au@Ag NPs contained less content of silver, but exhibited higher antibacterial activity than Ag NPs, indicating that Ag^+ is not the main contributor to highly effective antibacterial activity, though the ions definitely had impact on the overall bactericidal activity.[34] Pure Ag NPs have been reported to easily oxidize and aggregate in air, which often leads to significant reduction of antibacterial activity.[36] We then performed the stability test using Ag NPs and Au@Ag-2 NPs, two types of NPs were stored in light for 2 days and the UV-Vis spectra were measured. It can be noticed that the absorption peak of Ag NPs at 400 nm shifted to 417 nm with a large decrease in intensity, suggesting aggregation of Ag NPs (Fig. S5, ESI†). By contrast, the UV-Vis spectra of the Au@Ag-2 NPs changed little when stored in light for 2 days. Therefore, the Au@Ag-2 NPs are much more stable and resistant to oxidation and/or aggregation than pure Ag NPs. As we speculated, it is the outstanding stability that endows Au@Ag NPs with an excellent and a long-term antibacterial activity (Fig. S6, ESI†). Another probable reason for enhanced antibacterial activity of Au@Ag NPs may be correlated with the unique physicochemical structure of core–shell NPs. Besides, the electronic ligand effect in bimetallic NPs and the high free energy of the surface Ag atoms have been attributed to the synergistic effect with Au@Ag NPs.[29,37]

Disruption of bacterial cell membrane by Au@Ag NPs

To investigate the relationship between Au@Ag NPs and bacterial cell membrane damage, *E. coli* cells, after being treated with NPs and stained with SYTO9 and PI, were observed under confocal fluorescence microscopy. The green fluorescent dye SYTO9 stains both live and dead bacteria; but the red dye propidium iodide (PI) penetrates through only the ruptured membranes of the dead cells. Thus, the differences between the two-dye images have been widely used to distinguish dead and live bacteria and determine the integrity of the bacterial cell membranes.[38] As shown in Fig. 4, the untreated *E. coli* was stained in only green color, indicating cells were intact and in living state. However, *E. coli* cells treated with either Ag NPs or Au@Ag NPs also showed red color in addition to green color, suggesting either Ag NPs or Au@Ag NPs can affect the cell membrane integrity or disrupt bacterial cell membrane. It should be noticed that the fluorescent density of PI-stained *E. coli* cells relative to SYTO9-stained cells in the Au@Ag NPs treatment appeared much higher than that in the Ag NPs treatment, demonstrating that the Au@Ag core–shell structure

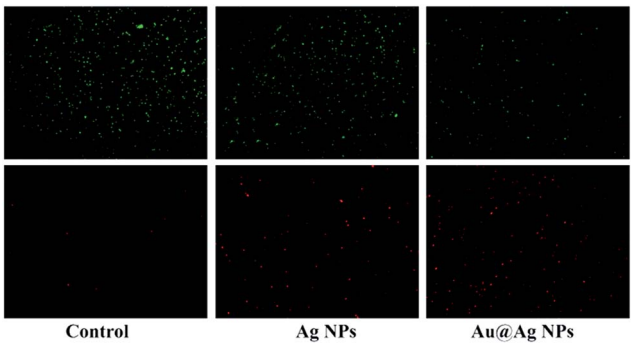

Fig. 4 Fluorescence microscopy images of *E. coli* before and after treatment with Ag NPs and Au@Ag-2 NPs followed by staining with SYTO9 (green) and PI (red).

result in more dead bacterial cells and can enhance antimicrobial activity of Ag NPs. SEM images shown that the morphology of *E. coli* cells after treatment with Au@Ag NPs was significant changed and exhibited obvious fragmentary pieces (Fig. 5), also demonstrating that Au@Ag NPs can damage the outer membrane of *E. coli*.

Cytotoxicity of gold@silver core–shell nanoparticles

Besides the antibacterial activities, the biocompatibility of Au@Ag NPs is another important factor in practical applications, in order to assess the toxicity effects of the nanoparticles on the cells, human neuroblastoma cell line (SH-SY5Y) was treated with various NPs at different concentration (Fig. 6). Based on a minimum cell viability of 70%,[30] Ag NPs is considered to be cytotoxic at ≥10 μg mL^{-1}, which is similar to the previous report that Ag NPs exhibited a significant cytotoxicity at >5.0 μg mL^{-1} to HepG2.[39] However, at the same total metal ion concentration, Au@Ag NPs were more compatible than pure Ag NPs, even at a concentration up to 80 μg mL^{-1}, we did not observe significant cytotoxicity of Au@Ag NPs to SH-SY5Y. Besides, for three types of Au@Ag NPs with different shell thickness, the order of the cytotoxicity of the core–shell NPs to SH-SY5Y cell is: Au@Ag-1 < Au@Ag-2 < Au@Ag-3, indicating that the high amount of silver is the main reason for the toxicity of Au@Ag NPs. Even so, 99% of SH-SY5Y cells remained viable after treated with 5 μg mL^{-1} Au@Ag-2 NPs for 24 h. These results demonstrated that the engineered Au@Ag NPs can inhibit the growth of bacteria, at the meantime, keep a great

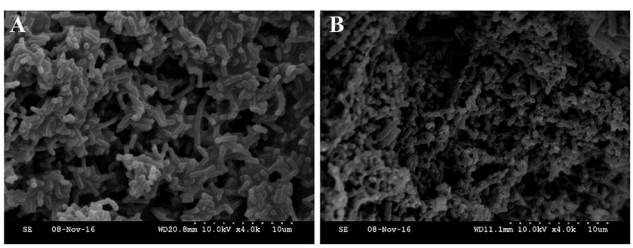

Fig. 5 Scanning electron microscope (SEM) images of *E. coli* before (A) and after (B) treatment with Au@Ag-2 NPs for 24 h.

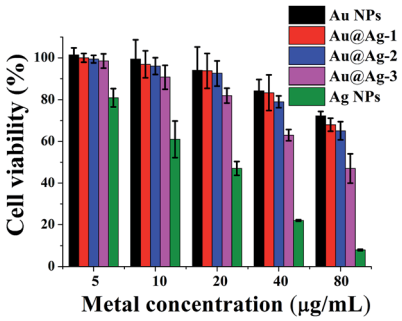

Fig. 6 Cell viability assay of SH-SY5Y cell lines treated with various NPs at different concentrations for 24 h. Error bars represent the standard deviations ($n = 4$).

biocompatibility with human cells. We speculated that the two distinct influences of Au@Ag NPs on bacteria and human cells were attributed to the different trace of Au@Ag NPs in the mitochondria of the cells. It has been demonstrated that NPs can interact with different protein and lead to no/irreversible damage to the DNA depending on their nanostructures.[25] This interesting results opens up the road for further researches on the effect of core–shell NPs at the single molecule level.

Conclusions

In summary, we synthesized Au@Ag NPs with varying Ag shell thickness, and investigated the influence of the shell thickness on the antibacterial activity and the cytotoxicity. Our data shown that among three thickness of NPs, the Au@Ag NPs with the shell thickness of 5 nm exhibited the strongest antibacterial activity with great biocompatibility with human cells. Most importantly, compared with individual Ag NPs and the simple mixture of Au and Ag NPs, bimetallic Au@Ag NPs with remarkable stability and a long-term antibacterial efficiency while possessed synergistically enhanced antibacterial activity against both Gram-negative and Gram-positive bacteria, even at a lower silver concentration. The result of fluorescence microscope and SEM images demonstrated that Au@Ag NPs can cause cell death by affecting the cell membrane integrity or causing cell membrane disruption. Given these advantages, we expect that Au@Ag NPs could be a promising candidate as a new bactericide in clinical and environmental applications.

Experimental section

Materials

Gold tetrachloroaurate trihydrate ($HAuCl_4$), sodium citrate, sodium ascorbate, sodium borohydride ($NaBH_4$), and poly(vinyl pyrrolidone) (PVP) were purchased from Sigma-Aldrich (Shanghai, China). Silver nitrate ($AgNO_3$) and K_2CO_3 were purchased from Xilong Chemical Ltd (Shantou, China). Tannic acid was purchased from Ryon Biological Technology Ltd (Shanghai, China). Broth medium, Eosin-Methylene Blue agar (EMB), and Baird–Parker agar base were purchased from Hope Bio-technology Ltd (Qingdao, China). LIVE/DEAD®BacLight™ Bacterial Vibility Kit was purchased from invitrogen Ltd (America). The human neuroblastoma cell lines (SH-SY5Y) were supplied by Shengxing Biological Ltd (Nanjing, China). *S. aureus* (CMCC(B)26003) and *E. coli* (ATCC25922) were obtained from Huankai microbial sci. & tech. Co., Ltd (Guangdong, China). All other chemicals and reagents were obtained from either Sigma-Aldrich (Shanghai, China) or Sinopharm Chemical Reagent Ltd (Beijing, China).

Synthesis of silver nanoparticles

Silver nanoparticles were synthesized using a standard procedure by reduction of silver nitrate.[40] Ag NPs with a diameter of 10 ± 3 nm were synthesized following the previously described method with some modifications. Briefly, 0.6 g of $NaBH_4$ was dissolved in 20 mL of distilled water (ice-cold), and then 5 mL of 1% poly(vinyl pyrrolidone) (PVP) was added as stabilizer (protecting agent). The solution was kept in a water-ice bath with high-speed stirring. Next, 5 mL of 1% PVP and 5 mL of 10 mM $AgNO_3$ were added to the solution prepared beforehand simultaneously by two constant-flow pumps at the rate of 30 mL h^{-1}. The final mixture was kept at 80 °C for 3 h to remove the unreacted $NaBH_4$. The finished sample was yellow and was stored at 4 °C.

Synthesis of gold nanoparticles

Au NPs were synthesized according to a previously reported procedure.[30] Au NPs (10 ± 2 nm) were synthesized by sodium citrate–tannin reduction. First, 1 mL of $HAuCl_4$ (1% by weight) was added into 79 mL of Millipore-Q water under stirring; the mixture was prepared as solution A. Second, 4 mL of sodium citrate (1% by weight), 0.1 mL of tannic acid (1% by weight), and 0.1 mL of K_2CO_3 (25 mM) were added into 15.8 mL of Millipore-Q water; the sample was mixed under stirring and named as solution B. Third, solutions A and B were separately heated to 60 °C for 30 min, and then solution B was quickly added into solution A under high-speed stirring. The solution was kept at 60 °C for 30 min until the color turned reddish orange and stable. Then the reddish orange solution was cooled to room temperature and stored at 4 °C.

Synthesis of gold@silver core–shell nanoparticles

Au@Ag NPs were prepared according to the procedure with some modification.[31] 50 μL of 5-fold concentrated Au NPs were dispersed into a solution containing 200 μL Millipore-Q water, 100 μL 1% PVP, and 50 μL 0.1 M sodium ascorbate. Different concentrations (3.5 mM, 7 mM, or 15 mM) of 10 μL $AgNO_3$ solution were added and synthesized nanoparticles were named as Au@Ag-1, Au@Ag-2, and Au@Ag-3 NPs, respectively. The reaction solution was shaken for 3 h at room temperature and then was centrifuged at 12 000 rpm for 10 min. The precipitate was washed three times and resuspended in Millipore-Q water.

Antimicrobial activity assays

S. aureus (CMCC(B)26003) and *E. coli* (ATCC25922) were cultured in broth medium in a shaking incubator at 37 °C overnight and the bacteria were harvested by centrifugation at 6000 rpm for 10 min at 4 °C and washed with sterile PBS.

The antibacterial activities of nanoparticles against *E. coli* and *S. aureus* were evaluated using a cell counting method. Pre-prepared nanomaterials (1.2–5 μg mL^{-1}) were added to bacteria (10^6 CFU mL^{-1}) and incubated at 37 °C with shaking at 200 rpm for 24 h. A 0.9% NaCl solution with bacteria was used as the positive control. The samples were diluted serially 10-fold before spotting onto Baird–Parker and EMB agar plates. After an overnight incubation at 37 °C, the CFUs were counted and used to determine cell survival. The dead bacterial was calculated as $(A - B)/A \times 100$ (where A is the number of surviving bacteria colonies in the control and B is that in the sample). Every experiment was repeated four times.

The growth curve was determined by measuring the time evolution of the optical density (OD_{600}). *S. aureus* and *E. coli* (10^6 CFU mL^{-1}) in the broth medium were incubated with 5 μg mL^{-1} Au@Ag NPs, respectively. The mixture of sterile water and bacterial solution was prepared as the control experiment. The bacterial growth rates were determined over a predefined time course by measuring the optical density (OD) at 600 nm by a UV-Vis spectrophotometer (UV-2600, Shimadzu).

For the minimum inhibitory concentration (MIC), bacterial cells were suspended in sterile broth medium to obtain a concentration of 10^6 CFU mL^{-1}. Then, each type of nanoparticles (Au NPs, Ag NPs, Au@Ag-2 NPs and the mixture of Au and Ag) was added to bacteria solutions and shaken at 37 °C for 24 h. Each NPs sample was tested at three times for each concentration along with triplicate positive (broth and bacteria) and negative (broth) controls. The lowest concentration at which there was no visual turbidity was taken as the MIC value of NPs.

Measurement of ion release

5 μg mL^{-1} nanoparticles were added to 10^6 CFU mL^{-1} *E. coli* and incubated at 37 °C. After certain time, the mixture was centrifuged at 15 000 rpm for 20 min at 4 °C to remove the bacterial cells and nanoparticles. The concentration of Ag^+ in the supernatant was determine by inductively coupled plasma mass spectrometry (ICP-MS) (Bruker-M90).

Live/dead bacterial assay

Live/dead bacterial assay was carried out to examine the effect of nanoparticles on the integrity of bacterial cell membranes.[41] 10 μg mL^{-1} Au@Ag NPs were added to 10^7 CFU mL^{-1} bacterial cells, the mixture was incubated at 37 °C for 24 h. Then the solutions were mixed with 0.5 mL of dye solution containing 1 μM SYTO9 and 5 μM propidium iodide (PI) for 20 min at room temperature. The bacteria cells were imaged using a confocal laser scanning microscope (TCS-SP2, Leica, Germany).

Cytotoxicity assay

The cell viability of human neuroblastoma cell line (SH-SY5Y) treated with each nanoparticles was measured using an MTT assay.[42] 100 μL of cells solution was added into a 96-well plate at a density of 5000 cells per plate and incubated at 37 °C, 5% CO_2 for 24 h. Then, cells were treated with various concentrations of each NPs solution and incubated for an additional 24 h. In parallel, cells with the addition of water served as negative controls. Then, 50 μL 0.5 mg mL^{-1} MTT bromide aqueous solution was added to each well of a 96-well plate. Following 4 h incubation, the medium was removed and formazan crystals were solubilized by incubation in 100 μL of DMSO for 10 min. Finally, the absorbance of each well was measured at a wavelength of 570 nm on a microplate reader (Synergy HT, BIO-TEK). The percent of cell viability was determined by the absorbance of the test sample divided by the absorbance value of the positive control.

Acknowledgements

This work is financially supported by the National Natural Science Foundation of China (Grants 31601569), the Fundamental Research Funds for the Central Universities (Grants KJQN201731), the China Postdoctoral Science Foundation (Grants 2016M600420), and the National Science & Technology Pillar Program (Grants 2015BAD16B05).

References

1 D. M. Eby, N. M. Schaeublin, K. E. Farrington, S. M. Hussain and G. R. Johnson, *ACS Nano*, 2009, **3**, 984–994.
2 J. B. Fei, J. Zhao, C. L. Du, A. H. Wang, H. Zhang, L. R. Dai and J. B. Li, *ACS Nano*, 2014, **8**, 8529–8536.
3 B. Le Ouay and F. Stellacci, *Nano Today*, 2015, **10**, 339–354.
4 O. Pandoli, R. D. S. Martins, E. C. Romani, S. Paciornik, M. Mauricio, H. D. L. Alves, F. V. Pereira-Meirelles, E. L. Luz, S. M. L. Koller, H. Valiente and K. Ghavami, *RSC Adv.*, 2016, **6**, 98325–98336.
5 I. Sondi and B. Salopek-Sondi, *J. Colloid Interface Sci.*, 2004, **275**, 177–182.
6 X. Yang, A. P. Gondikas, S. M. Marinakos, M. Auffan, J. Liu, H. Hsu-Kim and J. N. Meyer, *Environ. Sci. Technol.*, 2012, **46**, 1119–1127.
7 G. A. Sotiriou, A. Meyer, J. T. Knijnenburg, S. Panke and S. E. Pratsinis, *Langmuir*, 2012, **28**, 15929–15936.
8 J. Y. Liu, D. A. Sonshine, S. Shervani and R. H. Hurt, *ACS Nano*, 2010, **4**, 6903–6913.
9 A. Taglietti, Y. A. Diaz Fernandez, E. Amato, L. Cucca, G. Dacarro, P. Grisoli, V. Necchi, P. Pallavicini, L. Pasotti and M. Patrini, *Langmuir*, 2012, **28**, 8140–8148.
10 J. A. Lemire, J. J. Harrison and R. J. Turner, *Nat. Rev. Microbiol.*, 2013, **11**, 371–384.
11 A. Ivask, A. Elbadawy, C. Kaweeteerawat, D. Boren, H. Fischer, Z. Ji, C. H. Chang, R. Liu, T. Tolaymat, D. Telesca, J. I. Zink, Y. Cohen, P. A. Holden and H. A. Godwin, *ACS Nano*, 2014, **8**, 374–386.
12 S. George, S. Lin, Z. Ji, C. R. Thomas, L. Li, M. Mecklenburg, H. Meng, X. Wang, H. Zhang, T. Xia, J. N. Hohman, S. Lin, J. I. Zink, P. S. Weiss and A. E. Nel, *ACS Nano*, 2012, **6**, 3745–3759.
13 O. Bar-Ilan, R. M. Albrecht, V. E. Fako and D. Y. Furgeson, *Small*, 2009, **5**, 1897–1910.
14 S. Kittler, C. Greulich, J. Diendorf, M. Koller and M. Epple, *Chem. Mater.*, 2010, **22**, 4548–4554.

15 J. Song, H. Kim, Y. Jang and J. Jang, *ACS Appl. Mater. Interfaces*, 2013, **5**, 11563–11568.
16 I. Ocsoy, M. L. Paret, M. A. Ocsoy, S. Kunwar, T. Chen, M. X. You and W. H. Tan, *ACS Nano*, 2013, **7**, 8972–8980.
17 A. Naskar, S. Bera, R. Bhattacharya, P. Saha, S. S. Roy, T. Sen and S. Jana, *RSC Adv.*, 2016, **6**, 88751–88761.
18 J. L. Chen, M. L. Mei, Q. L. Li and C. H. Chu, *RSC Adv.*, 2016, **6**, 104025–104035.
19 K. K. Haldar, S. Kundu and A. Patra, *ACS Appl. Mater. Interfaces*, 2014, **6**, 21946–21953.
20 J. Xu, A. R. Wilson, A. R. Rathmell, J. Howe, M. Chi and B. J. Wiley, *ACS Nano*, 2011, **5**, 6119–6127.
21 S. Liu, Z. Sun, Q. Liu, L. Wu, Y. Huang, T. Yao, J. Zhang, T. Hu, M. Ge, F. Hu, Z. Xie, G. Pan and S. Wei, *ACS Nano*, 2014, **8**, 1886–1892.
22 L. Tang, S. Li, L. Xu, W. Ma, H. Kuang, L. Wang and C. Xu, *ACS Appl. Mater. Interfaces*, 2015, **7**, 12708–12712.
23 W. Feng, X. Zhou, W. Nie, L. Chen, K. Qiu, Y. Zhang and C. He, *ACS Appl. Mater. Interfaces*, 2015, **7**, 4354–4367.
24 L. Zeng, Y. Pan, S. Wang, X. Wang, X. Zhao, W. Ren, G. Lu and A. Wu, *ACS Appl. Mater. Interfaces*, 2015, **7**, 16781–16791.
25 M. Mahmoudi and V. Serpooshan, *ACS Nano*, 2012, **6**, 2656–2664.
26 C. Fasciani, M. J. Silvero, M. A. Anghel, G. A. Arguello, M. C. Becerra and J. C. Scaiano, *J. Am. Chem. Soc.*, 2014, **136**, 17394–17397.
27 X. Dai, Z. Fan, Y. Lu and P. C. Ray, *ACS Appl. Mater. Interfaces*, 2013, **5**, 11348–11354.
28 H. Alishah, S. Pourseyedi, S. E. Mahani and S. Y. Ebrahimipour, *RSC Adv.*, 2016, **6**, 73197–73202.
29 M. Banerjee, S. Sharma, A. Chattopadhyay and S. S. Ghosh, *Nanoscale*, 2011, **3**, 5120–5125.
30 J. D. Padmos, M. Langman, K. MacDonald, P. Comeau, Z. Yang, M. Filiaggi and P. Zhang, *J. Phys. Chem. C*, 2015, **119**, 7472–7482.
31 Y. Zhao, L. Xu, W. Ma, L. Wang, H. Kuang, C. Xu and N. A. Kotov, *Nano Lett.*, 2014, **14**, 3908–3913.
32 R. Wang, Y. Yao, M. Shen and X. Wang, *Colloids Surf., A*, 2016, **492**, 263–272.
33 V. R. Chelli and A. K. Golder, *RSC Adv.*, 2016, **6**, 95483–95493.
34 Z. M. Xiu, Q. B. Zhang, H. L. Puppala, V. L. Colvin and P. J. Alvarez, *Nano Lett.*, 2012, **12**, 4271–4275.
35 H. Y. Wang, X. W. Hua, F. G. Wu, B. Li, P. Liu, N. Gu, Z. Wang and Z. Chen, *ACS Appl. Mater. Interfaces*, 2015, **7**, 7082–7092.
36 M. Lv, S. Su, Y. He, Q. Huang, W. Hu, D. Li, C. Fan and S. T. Lee, *Adv. Biomater.*, 2010, **22**, 5463–5467.
37 Y. M. Zhai, L. Han, P. Wang, G. P. Li, W. Ren, L. Liu, E. K. Wang and S. J. Dong, *ACS Nano*, 2011, **5**, 8562–8570.
38 Q. Cai, Y. Gao, T. Gao, S. Lan, O. Simalou, X. Zhou, Y. Zhang, C. Harnoode, G. Gao and A. Dong, *ACS Appl. Mater. Interfaces*, 2016, **8**, 10109–10120.
39 K. Kawata, M. Osawa and S. Okabe, *Environ. Sci. Technol.*, 2009, **43**, 6046–6051.
40 W. Yan, L. Xu, C. Xu, W. Ma, H. Kuang, L. Wang and N. A. Kotov, *J. Am. Chem. Soc.*, 2012, **134**, 15114–15121.
41 I. Irwansyah, Y. Q. Li, W. Shi, D. Qi, W. R. Leow, M. B. Tang, S. Li and X. Chen, *Adv. Biomater.*, 2015, **27**, 648–654.
42 M. C. Wu, A. R. Deokar, J. H. Liao, P. Y. Shih and Y. C. Ling, *ACS Nano*, 2013, **7**, 1281–1290.